Geomicrobiology Journal, 21:415–429, 2004

ISSN: 0149-0451 print / 1362-3087 online
DOI: 10.1080/01490450490485845

Taylor & Francis
Taylor & Francis Group

Four-Hundred-and-Ninety-Million-Year Record of Bacteriogenic Iron Oxide Precipitation at Sea-Floor Hydrothermal Vents

Crispin T. S. Little,[1] Sarah E. J. Glynn,[2] and Rachel A. Mills[2]
[1]*School of Earth Sciences, University of Leeds, Leeds, United Kingdom*
[2]*School of Ocean and Earth Science, Southampton Oceanography Centre, University of Southampton, Southampton, United Kingdom*

Fe oxide deposits are commonly found at hydrothermal vent sites at mid-ocean ridge and back-arc sea floor spreading centers, seamounts associated with these spreading centers, and intra-plate seamounts, and can cover extensive areas of the seafloor. These deposits can be attributed to several abiogenic processes and commonly contain micron-scale filamentous textures. Some filaments are cylindrical casts of Fe oxyhydroxides formed around bacterial cells and are thus unquestionably biogenic. The filaments have distinctive morphologies very like structures formed by neutrophilic Fe oxidizing bacteria. It is becoming increasingly apparent that Fe oxidizing bacteria have a significant role in the formation of Fe oxide deposits at marine hydrothermal vents. The presence of Fe oxide filaments in Fe oxides is thus of great potential as a biomarker for Fe oxidizing bacteria in modern and ancient marine hydrothermal vent deposits. The ancient analogues of modern deep-sea hydrothermal Fe oxide deposits are jaspers. A number of jaspers, ranging in age from the early Ordovician to late Eocene, contain abundant Fe oxide filamentous textures with a wide variety of morphologies. Some of these filaments are like structures formed by modern Fe oxidizing bacteria. Together with new data from the modern TAG site, we show that there is direct evidence for bacteriogenic Fe oxide precipitation at marine hydrothermal vent sites for at least the last 490 Ma of the Phanerozoic.

Keywords bacteriogenic iron oxides, TAG, hydrothermal vents, jaspers

Received 10 October 2003; accepted 14 May 2004.

This research has been funded in part by grants from the Natural Environment Research Council (GR3/10903 and GT4/00/247), INTAS, and NASA Astrobiology Initiative. We thank Tor Grenne (Geological Survey of Norway) and John Slack (USGS) for providing the photomicrographs of the Løkken area jaspers, and two anonymous reviewers and David Emerson for comments on an earlier draft of the paper. CTSL wishes to thank the following colleagues: Nathan Yee, Richard Herrington, Valeriy Maslennikov, Rachel Haymon, and Bruce Runnegar. SEJG wishes to thank Bob Jones, John Ford, and Richard Pearce.

Address correspondence to Crispin T. S. Little, School of Earth Sciences, University of Leeds, Leeds LS2 9JT, UK. E-mail: c.little@earth.leeds.ac.uk

INTRODUCTION

Fe oxide deposits are commonly found at hydrothermal vent sites at mid-ocean ridge and back-arc sea floor spreading centers, seamounts associated with these spreading centers, and intraplate seamounts (e.g., Barrett, Taylor, and Lugowski 1987; Alt 1988; Binns et al. 1993; Hekinian et al. 1993; Stoffers et al. 1993; Bogdanov et al. 1998; Iizasa et al. 1998; Halbach, Halbach, and Lüders 2002). The formation of such deposits can be attributed to several abiogenic processes: sedimentation from hydrothermal plumes (e.g., Barrett et al. 1987; Mills, Elderfield, and Thomson 1993); in situ precipitation from diffuse low-temperature flow through sediments (e.g., Koski et al. 1985; Alt 1988), typically 20–100°C (e.g., Mills et al. 1996; Bau and Dulski 1999; Severmann, Mills, Palmer, and Fallick 2004); material derived from low-temperature vent chimneys, typically 2–50°C (e.g., Alt, Lonsdale, Haymon, and Muehlenbachs 1987; Herzig et al. 1988; James and Elderfield 1996); and the products of Fe-rich sulfide oxidation (e.g., Alt 1988; Binns et al. 1993; Mills et al. 1993). The mineralogy of these Fe oxide deposits is dominated by poorly ordered Fe oxyhydroxides (Two-XRD-line ferrihydrite and goethite), often with significant amounts of amorphous silica (up to 73 wt%) and Mn (up to 14 wt%) (Alt 1988; Juniper and Fouquet 1988; Binns et al. 1993; Hekinian et al. 1993; Stoffers et al. 1993; Fortin, Ferris, and Scott 1998; Iizasa et al. 1998; Boyd and Scott 2001; Emerson and Moyer 2002; Kennedy, Scott, and Ferris 2003a).

Microbial activity is thought to play a role in the formation of marine hydrothermal Fe oxide deposits (Alt et al. 1987; Juniper and Fouquet 1988; Hannington and Jonasson 1992; Juniper and Sarrazin 1995; Emerson and Moyer 2002; Edwards et al. 2003a, 2003b). Fe-oxidizing microbes are capable of influencing the growth and dissolution of a number of minerals by exerting control over reaction kinetics and pathways. However, relationships between Fe oxide-deposits and extant microbial populations are poorly constrained because of difficulties in distinguishing authigenic microfossils from abiogenic artifacts,

Table 1
Occurrences of filamentous structures in marine hydrothermal deposits

Location	Depth (m)	Deposit type	Filament morphologies	Reference
Magic Mountain deposit, Explorer Ridge, NE Pacific	1,794–1,808	Si and Mn-rich Fe oxides, Fe silicates	Circular and oval holes	Fortin et al. 1998
Philosopher Vent, Explorer Ridge		Amorphous silica and Fe-oxide	Hyphae-like filament networks, long branching filaments, hollow filaments 1–2-μm diameter	Juniper and Fouquet 1988
Main Endeavour segment, Juan de Fuca Ridge (JdFR) NE Pacific	2,400	Various metal sulfides	Irregularly twisted branching filaments, coiled and vibroid-shaped cells, and chains of nanospheres.	Edwards et al. 2003a
Middle Valley segment, JdFR		Metal sulfide unspecified	Twisted, dendritic Fe-oxides, straight bundles of filaments, braided filaments	Edwards et al. 2003b
Axial Volcano, JdFR 46°N, 130°W	1,500	Fe-oxides unspecified	Spirals, sheaths, PV-1	Kennedy et al. 2003a, 2003b, 2003c
21° 30′N East Pacifiic Rise (EPR)		Fragment of inactive oxide chimney	Hollow filaments	Juniper and Fouquet 1988
Red Sea Mount, EPR, 21°N	1,940	Not specified; soft oxide muds	Fe-oxide spirals, flat twisted ribbons; Short multibranching filaments	Alt 1988; Juniper and Fouquet 1988
Seamount 5, EPR, 13°N	1,000	amorphous Fe oxides and nontronite	Twisted filaments	Alt 1988
EPR, 12° 50′N		Chimney fragment; not specified	Branching filaments	Juniper and Fouquet 1988
Galapagos Rift, 0°N, 85°W	2,550	Nontronite	Filaments, tubes and sheaths	Köhler et al. 1994
Loihi Seamount, Hawaii	1,200		Sheaths, twisted filaments, extensive bacterial mats	Emerson and Moyer 2002
Franklin Seamount, Woodlark Basin, SW Pacfic	2,143–2,366	Fe-Si-Mn oxyhydroxides	Branching, bunched, braided filaments	Binns et al. 1993; Bogdanov et al. 1997; Boyd and Scott 2001
Coriolis Troughs, SW Pacific	1,100–1,500	Fe-Si oxyhydroxides	Filamentous web like networks Hollow tubes	Iizasa et al. 1998
Mariana Trough, 18°N, 144°W	3,610	Nontronite	Filaments, tubes, and sheaths	Kohler et al. 1994
Meso Zone, Central Indian Ocean	2,870	Jasper	Dendritic filaments	Halbach et al. 2002
Knipovich Ridge, Mid Atlantic Ridge (MAR), 76°N			Twisted filaments	Thorseth et al. 2001
FAMOUS, MAR, 36° 57′N		From oxide mound unspecified	Clustered branching filaments	Juniper and Fouquet 1988
TAG, MAR, 26°N	3,650	Red and gray chert, not specified	Thread like cellular masses, chains of nanospheroids	Al-Hanbali and Holm 2002; Al-Hanbali et al. 2001
TAG	3,650	Moss agate	Branching dendritic Fe-oxides (assigned an abiogenic origin)	Hopkinson et al. 1998
Santorini, Mediterranean	2	Fe oxide-hydroxide	Sheaths, twisted filaments	Hanert 1973, 2002; Holm 1987

as the effects of diagenesis can lead to the loss of biogenic signatures. Although Fe-oxidizing bacteria are inferred to be ubiquitous in hydrothermal environments where there are sharp pH and redox gradients, and a fresh supply of Fe(II) in dissolved and particulate forms, their impact on Fe-oxidation at vent sites and their role in the formation of Fe oxide deposits remains unquantified.

Extensive sampling of hydrothermal vent sites over the last few decades has led to many observations of Fe oxide and silicified filamentous textures in low temperature Fe oxide-rich deposits (Table 1) and also in vent fluids (Halbach, Koschinsky, and Halbach 2001). The filaments are usually between 1 and 5 μm in diameter, and 10s to 100s μm long. Many have distinctive morphologies, including twisted ribbons, hollow sheaths and dendritic filaments (Alt 1988; Juniper and Fouquet 1988; Stoffers et al. 1993; Halbach et al. 2001; Thorseth et al. 2001; Boyd and Scott 2001; Emerson and Moyer 2002; Kennedy et al. 2003a, 2003b, 2003c). Several authors have noted the similarity of these morphologies with structures formed by neutrophilic Fe-oxidizing bacteria, including *Gallionella ferruginea*, which grows Fe encrusted twisted stalks (e.g., Hanert 1973, 2002), and *Leptothrix ochracea*, which forms Fe oxide encrusted sheaths (e.g., Emerson and Revsbech 1994). Although neither of these bacterial taxa have been conclusively identified (by culture or molecular analysis) from marine hydrothermal Fe oxide deposits, a novel strain of Fe-oxidizing bacterium (PV-1) has been cultured from the Loihi seamount vent site (Emerson and Moyer 2002). PV-1 grows slender (<1 μm diameter) Fe oxide filaments, very like filaments in natural samples from the seamount. Very similar sheathed and helical Fe oxide filaments have also been observed to form on sulfide surfaces at a low temperature vent within the Endeavour Vent Field, Juan de Fuca Ridge (JdFR) during in situ incubation experiments (Edwards et al. 2003a, 2003b). TEM and epiflourescence imaging has shown that some of the filaments described in the literature are cylindrical casts of Fe oxyhydroxides formed around bacterial cells (Fortin et al. 1998; Hanert 2002; Emerson and Moyer 2002; Kennedy et al. 2003a, 2003b, 2003c), and are thus unquestionably biogenic. However, most identification of microbial structures in natural samples is based on similarity in morphology of filaments, and there are problems associated with recognition of bacterial structures based on shape alone (e.g., Reysenbach and Cady 2001; García-Ruiz et al. 2002, 2003).

The extent to which precipitation and mediation of iron, silica and sulfate minerals is the result of the metabolic activity of the bacteria, or a more passive process where the functional groups on the bacterial surfaces react with positively charged ions, is unclear (e.g., Konhauser 1998; Banfield et al. 2000; Glasauer, Langley, and Beveridge 2001; Emerson and Moyer 2002; Kennedy et al. 2003a, 2003b, 2003c). Abiogenic processes are inferred to dominate oxidation of Fe(II) in hydrothermal plumes and at the seafloor where Fe(II) has a half life of <1 minute (Millero, Sotolongo, and Izaguirre 1987) and oxidation proceeds rapidly. However, abiogenic oxidation of Fe(II) proceeds extremely slowly in the lower pH ($\sim$6 pH), low oxygen ($O_2 \sim 1$ ml/l) environments present in the upper 10s of centimetres of hydrothermal deposits with Fe(II) half lives >5 days (Millero et al. 1987). This environment potentially provides the conditions for significant biological mediation of Fe(II) oxidation (Emerson and Moyer 2002). Demonstrating an association between bacteria and Fe oxidation is key to quantifying their role in the alteration of Fe-rich hydrothermal deposits. The presence of Fe oxide and silica coated filaments is of great potential as a biomarker for Fe oxidizing bacteria in modern and ancient hydrothermal vent deposits (Boyd and Scott 2001; Little and Thorseth 2002; Emerson and Moyer 2002; Kennedy et al. 2003a).

The ancient analogues of modern deep-sea hydrothermal Fe oxide deposits are jaspers. These are stratiform beds of hematitic chert volcanic rock sequences and are commonly associated with massive sulfide deposits (e.g., Duhig et al. 1992a, 1992b; Little et al. 1999; Davidson, Stolz, and Eggins 2001; Little and Thorseth 2002; Grenne and Slack 2003b); (Figure 1). Most authors suggest these jaspers were the product of low-temperature, diffuse hydrothermal venting because of their similarity to modern Fe oxide deposits (although see Grenne and Slack 2003a for an alternative explanation). However, jaspers differ from most modern Fe oxide deposits because (1) they contain a much greater percentage of silica (80–95 vol%) (Davidson et al. 2001; Grenne and Slack 2003b), and (2) the Fe oxides are present within the jaspers largely as hematite (rather than ferrihydrite and goethite), and the silica is present as chalcedony and/or quartz (rather than amorphous silica). The latter differences probably reflect the greater thermal maturity of these ancient deposits rather than different physicochemical regimes, as neither amorphous silica nor ferrihydrite are stable over long time scales, particularly when heated by low-grade metamorphism (e.g., Cornell and Schwertmann 1996; Boyd and Scott 2001). Jaspers also have very complex mineralogical textures indicating that they have matured from colloidal gels rich in silica and Fe (Duhig et al. 1992a, 1992b; Davidson et al. 2001; Grenne and Slack 2003a, 2003b).

Detailed examination of ten jaspers from various palaeotectonic settings ranging in age from the early Ordovician to the late Eocene has revealed abundant Fe oxide filamentous textures (Juniper and Fouquet 1988; Alt et al. 1992; Duhig et al. 1992a, 1992b; Little et al. 1999; Little and Thorseth 2002; Grenne and Slack 2003a, 2003b) (Table 2). Some of these filaments have distinctive morphologies, which have been tentatively linked to Fe-oxidizing bacteria, such as *Gallionella* spp. In this paper we review these jasper filament occurrences and present new data of filamentous textures from modern metalliferous sediments associated with the TAG hydrothermal area, MAR. We discuss the evidence for the biogenicity of these modern and ancient filaments, and in so doing show that there is very good evidence for bacteriogenic Fe oxide precipitation at deep-sea hydrothermal vent sites for the last 490 Ma of the Phanerozoic.

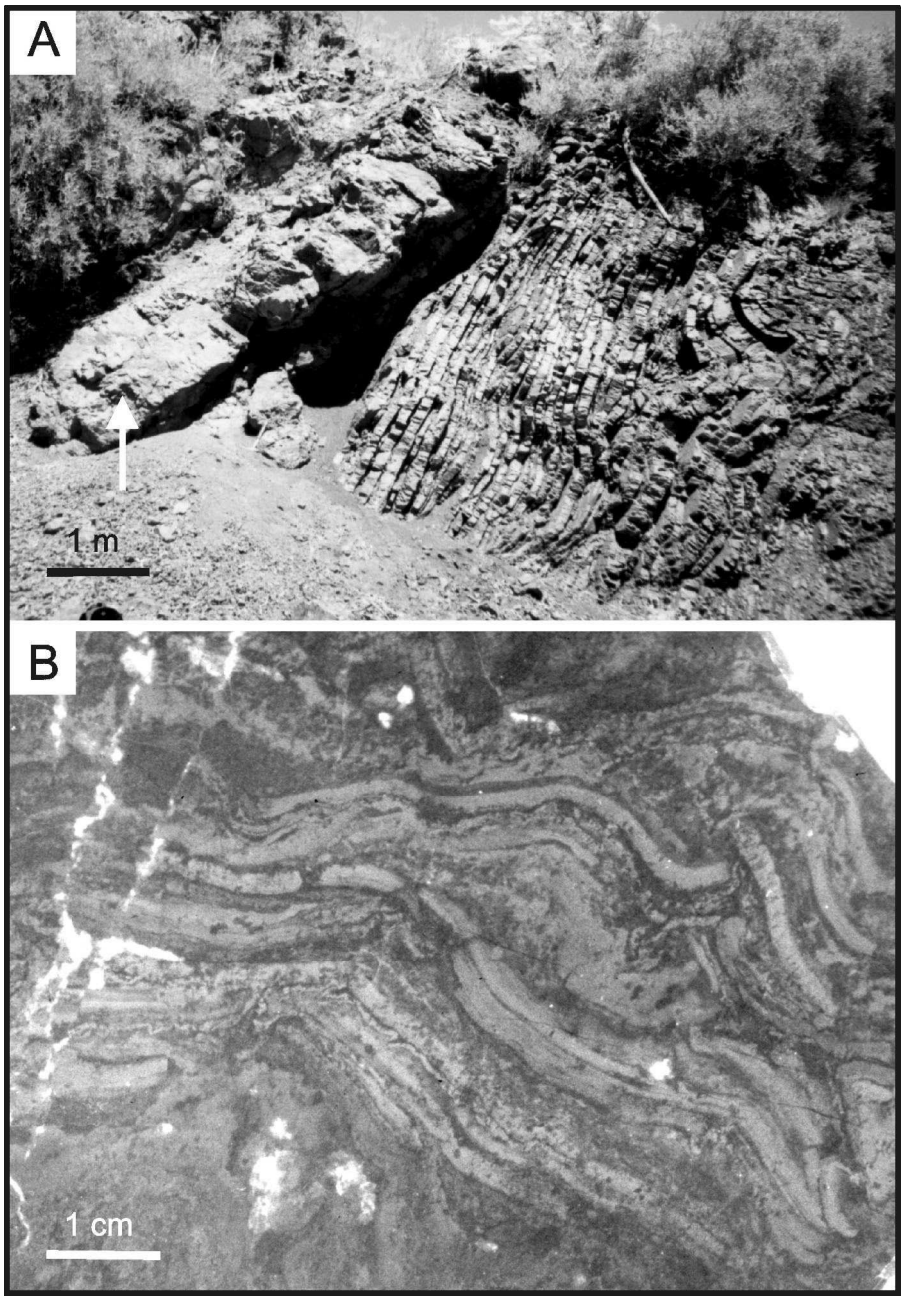

Figure 1. Jaspers in the field and hand specimen. (A) Arrow points to jasper bed lateral to the Figueroa sulfide deposit. To the right of the jasper bed is a sequence of radiolarian rich bedded cherts. (B) Polished hand specimen of Høydal jasper showing the Fe-rich and Fe-poor banding, disrupted in places.

MATERIALS AND METHODS

TAG Metalliferous Sediment Core

The TAG hydrothermal field occupies an area of ~25 km^2 at 26°N on the eastern side of the median valley of the Mid Atlantic Ridge (e.g., Rona et al. 1986). The TAG field comprises an active sulfide mound and two relict high temperature zones between 3,400 and 3,500 m water depth. The *Alvin* zone is a discontinuous, elongate group of several inactive sulfide mounds ~2 × 1 km (Rona et al. 1993). The TAG sediment core was collected from the periphery of the southern most mound within the *Alvin* relict high-temperature zone during RRS Charles Darwin cruise 102 (Palmer et al. 1996). The mound surface is covered by metalliferous sediments with standing and toppled inactive sulfide chimneys on the upper surface (Rona et al. 1993). The *Alvin* zone has been inactive and exposed to seawater for

Table 2
Jaspers with filaments

Jasper deposit and reference	Location	Age	Host rocks	Palaeotectonic setting
Barlo (Juniper and Fouquet 1988)	Luzon, Philippines	Late Eocene	Zambales Ophiolite; jasper associated with Barlo VMS deposit	Supra-subduction zone
Kambia (Little and Thorseth 2002)	Cyprus	Late Cretaceous (~91 Ma)	Basaltic pillow lavas of Troodos Ophiolite; jasper associated with Kambia VMS deposit	Supra-subduction zone
Troodos (Juniper and Fouquet 1988)	Cyprus	Late Cretaceous (~91 Ma)	Interpillow chert from Troodos Ophiolite	Supra-subduction zone
Coast Range Ophiolite (Juniper and Fouquet 1988)	California, USA	Late Jurassic	Interpillow chert from Coast Range Ophiolite	Supra-subduction zone fore-arc basin
ODP Core 129-801C-4R (Alt et al. 1992)	Pigafetta Basin, W. Pacific	Mid Jurassic (~165 Ma)	Pillow basalts	Mid-ocean ridge and ocean island
Figueroa (Little et al. 1999; Little and Thorseth 2002)	California, USA	Early Jurassic (~190 Ma)	Basaltic pillow lavas of Franciscan Complex; jasper associated with Figueroa VMS deposit	Mid-ocean ridge or ocean island
Ballynoe (Little and Thorseth 2002; Boyce et al. 2003)	Ireland	Early Carboniferous (~352 Ma)	Carbonates; jasper occurs within Ballynoe barite deposit	Intracratonic basin
Alexandrinka (Little and Thorseth 2002)	Chelyabinsk district, S. Urals, Russia	Mid Devonian (~390 Ma)	Rhyodacites; jasper associated with Alexandrinka VMS deposit	Island-arc
Mount Windsor Formation (Duhig et al. 1992a, 1992b)	Queensland, Australia	Early Ordovician (481–485 Ma)	Felsic volcanics of Mount Windsor Formation; some jaspers associated with Thalanga VMS deposit	Back-arc basin
Løkken area (Little and Thorseth 2002; Grenne and Slack 2003a, 2003b)	Trondheim region, Norway	Early Ordovician (~490 Ma)	Basaltic pillow lavas of Løkken ophiolite; jaspers associated with Løkken and Høydal VMS deposits	Back-arc basin

~40–50,000 years (Lalou et al. 1990). Downcore mineralogy was obtained from X-ray diffraction patterns of selected samples on a Philips PW 1730 automated powder diffractometer using Co-K_α radiation. Dry powder mounts were scanned between 2–60° at 0.2° 2θ/min. The detection limit for all minerals is 1%. Three polished thin sections, 30 μm thick, were prepared from a 10-cm-thick stripped section of alternating black and orange material, located at the top of a sulfidic layer at 75 cm depth. This section was impregnated with epoxy resin prior to sectioning. The polished thin sections were observed and photographed in transmitted and reflected light.

Jaspers

Table 2 gives location and background geological details of the ten jasper deposits from which filaments have been recorded. Table 3 gives mineralogical and morphological details of the jasper filaments. These jaspers were studied variously using optical microscopy, SEM, TEM, Laser Raman spectroscopy, electron microbe analysis and XRD, see Juniper and Fouquet (1988), Alt et al. (1992), Duhig et al. (1992a, 1992b), Little and Thorseth (2002), and Grenne and Slack (2003b) for details of methodology.

RESULTS

Filament Occurrence Within TAG Samples

XRD traces indicate that black layers are dominated by pyrite, with smaller quantities of chalcopyrite and sphalerite with minor covellite. Orange layers are predominantly composed of goethite with quartz, gypsum, and minor clays. Well-preserved hematitic and goethitic filaments were observed in all goethite and quartz-dominated layers, and are associated with an alteration mineral assemblage of gypsum, secondary pyrite, covellite, atacamite, and goethite. All the filaments are 1–10 μm in diameter and

Table 3
Jasper mineralogy and filament details

Jasper deposit	Bulk mineralogy	Filament mineralogy	Filament morphology and dimensions; d = diameter, l = length
Barlo	Pyritic chert	Fe oxide	Short, simply branching; d = 10 μm, l = up to 100 μm (estimated from Figure 4c, Juniper and Fouquet 1988)
Kambia	Quartz, chalcedony, hematite	Hematite	a) Curved, branching; d = up to 10 μm, l = up to 400 μm b) Branching dendrites; d = ~20 μm, l = up to 500 μm
Troodos	Chert	Fe oxide	Branching and straight; d = 10–30 μm, l = up to 1000 μm (estimated from Figure 4A, B, Juniper and Fouquet 1988)
Coast Range Ophiolite	Brecciated chert	Fe oxide	Short, simply branching; d = 10 μm, l = up to 60 μm (estimated from Figure 4D, Juniper and Fouquet 1988)
ODP Core 129–801C-4R	Quartz, Fe oxyhydroxide	Fe oxyhydroxide	a) Curved and branching; d = ~5 μm, l = 50–100 μm b) Double twisted spirals; d = ~5 μm, l = <200 μm
Figueroa	Quartz, hematite	Hematite	a) Curved or looped, some septate, some with terminal bulbs; d = 1.2–4.8 μm, l = up to 200 μm b) Branching dendrites; d = 6–24 μm, l = up to 800 μm
Ballynoe	Quartz, hematite, barite	Hematite	a) Branching, twisted and straight; d = 2–5 μm, l = up to 200 μm b) Branching dendrites; d = 5–30 μm, l = up to 2500 μm
Alexandrinka	Quartz, hematite	Hematite	Branching, straight; d = up to 10 μm, l = up to 300 μm
Mount Windsor Formation	Quartz, chalcedony, hematite	Hematite	a) Septate; d = ~10 μm b) Nonseptate; d = ~5 μm Both a) and b) show branching and reconnection c) Branching; d = 20–30 μm l = 1000–3000 μm
Løkken	Quartz, hematite; minor goethite and carbonate	Hematite	Type I, straight or curved; d = 3–10 μm, l = 20–100 μm Type II, branching networks; d = up to 25 μm, l = 30–300 μm

up to 250 μm in length, and occur cemented within silica and gypsum, or as noncemented meshes (Figures 2 and 3).

TAG Filament Morphologies

Dendritic branching structures dominate the morphology of filaments cemented in gypsum. In some instances, the filaments radiate from dense masses in the center of the gypsum crystals, forming dendritic structures (Figure 2A). Other gypsum-cemented examples show coiling and bundled filaments (Figure 2B). Sulfide minerals are often found within the gypsum crystals adjacent to the filaments. The morphology and occurrence of quartz-cemented filaments differs from those within gypsum in several respects. Branching forms are less frequent and commonly less densely packed, and the filament morphology is dominated by short rod-like filaments and longer, twisted

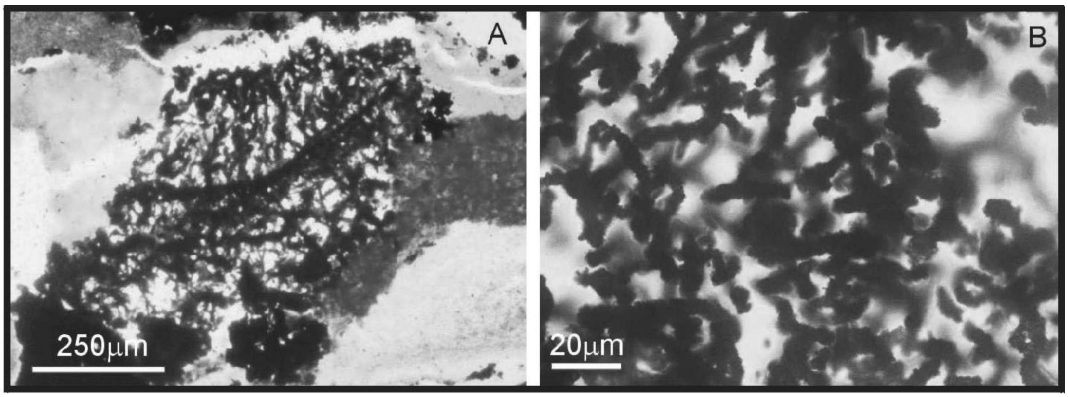

Figure 2. Transmitted light photomicrographs of filamentous structures in *Alvin* zone gypsum. (A) Filaments within euhedral gypsum crystal. (B) Bundled twisted filaments.

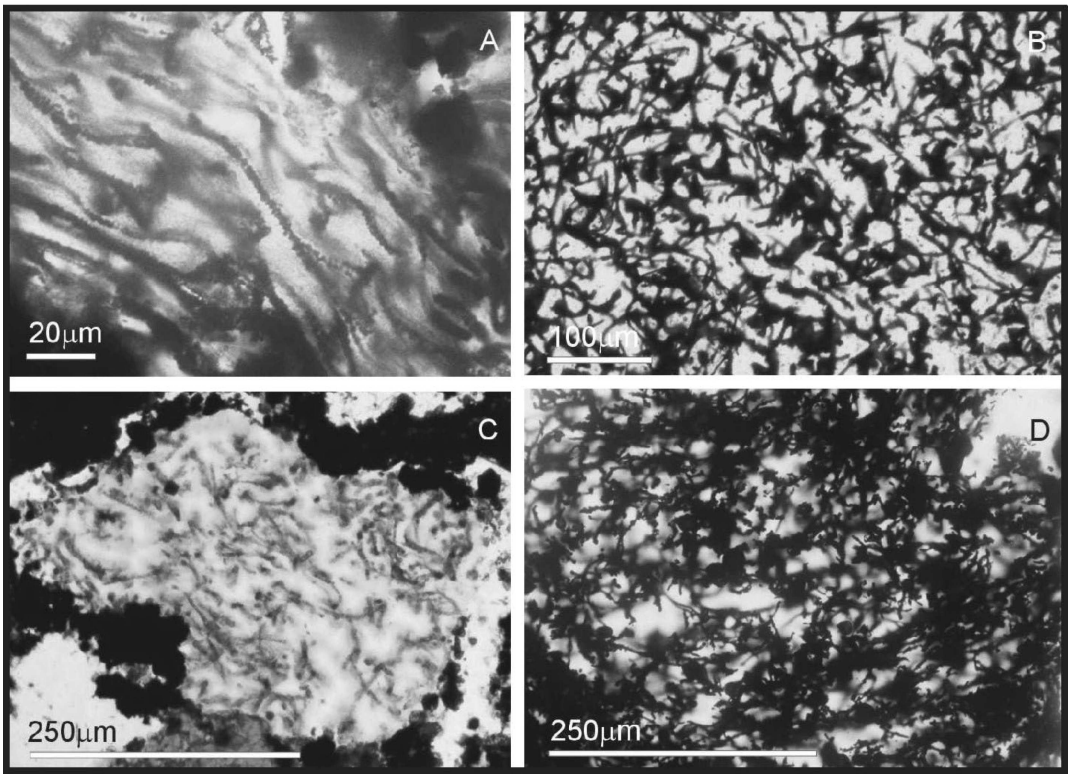

Figure 3. Transmitted light photomicrographs of filamentous structures in *Alvin* zone silica. (A) Long twisted goethite filaments showing directed growth lengthwise parallel to sedimentary layering. (B) Rod-like hematite filaments. (C) Branching filaments. (D) Mesh of twisted and rod-like filaments.

forms showing directed growth (Figure 3). In many cases, the apparent growth direction is parallel to the sedimentary laminae. The quartz-cemented filaments are commonly associated with chalcedony spherules that appear to have nucleated on the filaments, and in some cases the filaments cross cut the spherules. At high magnification using a light microscope some of the quartz cemented rod like hematite filaments appear to be tubes of hematite with blebs of goethite along their length. The non-cemented filaments are extremely fragile, form dense nets of interlocking branched filaments, and are always closely associated with sulfide minerals.

Filament Occurrence Within Jaspers

Filaments are not present throughout the jaspers but are concentrated in discrete laminae or irregular shaped, millimetric-scale domains, surrounded by Fe oxide-rich areas (principally hematite) with lesser proportions of silica minerals (chalcedony and/or quartz) (Figure 4). In all the jasper samples the filaments are paragenetically early and form up to 40 vol% of the laminae and domains in which they occur (Figure 4). All of the filaments are cemented by later silica phases, which can be chalcedony and/or quartz. The fact that filaments often cross quartz and chalcedony crystal boundaries proves that the silica mineralization postdates hematite filament formation, and the filaments are not grain boundary artifacts. In the Figueroa, Mount Windsor, ODP Core 129-801C-4R, and Løkken jaspers the filaments are associated with small spherules of cryptocrystalline quartz and/or hematite of various size (<10 μm diameter in Løkken) (Figure 4F). The timing of formation of these spherules is ambiguous (Grenne and Slack 2003b), but at least some are paragenetically of the same age as the filaments (Juniper and Fouquet 1988).

Jasper Filament Morphologies

The jasper filaments have a wide range of sizes and morphologies (Table 3) (Figure 5), but can be separated into small types and large types based on their size, morphology and degree of mineralization. However, these types are not entirely distinct because, as is discussed later, in some rare cases the former can be seen to give rise directly to the latter. The small filaments are between 1.2 and around 10 μm in diameter and are up to 200 μm long. Most of them have constant diameters along their length, but some taper, particularly distally of any branching points. They have a wide variety of morphologies: some are straight (Figure 6G, H), but the majority are curved (Figure 6C) and/or show irregular branching (Figure 6A, B, D, H, I). A few of the filaments in the Figueroa and Mount Windsor jaspers have internal septae (Figure 6F; Duhig et al. 1992a, Figure 3B), and some of the Figueroa filaments have

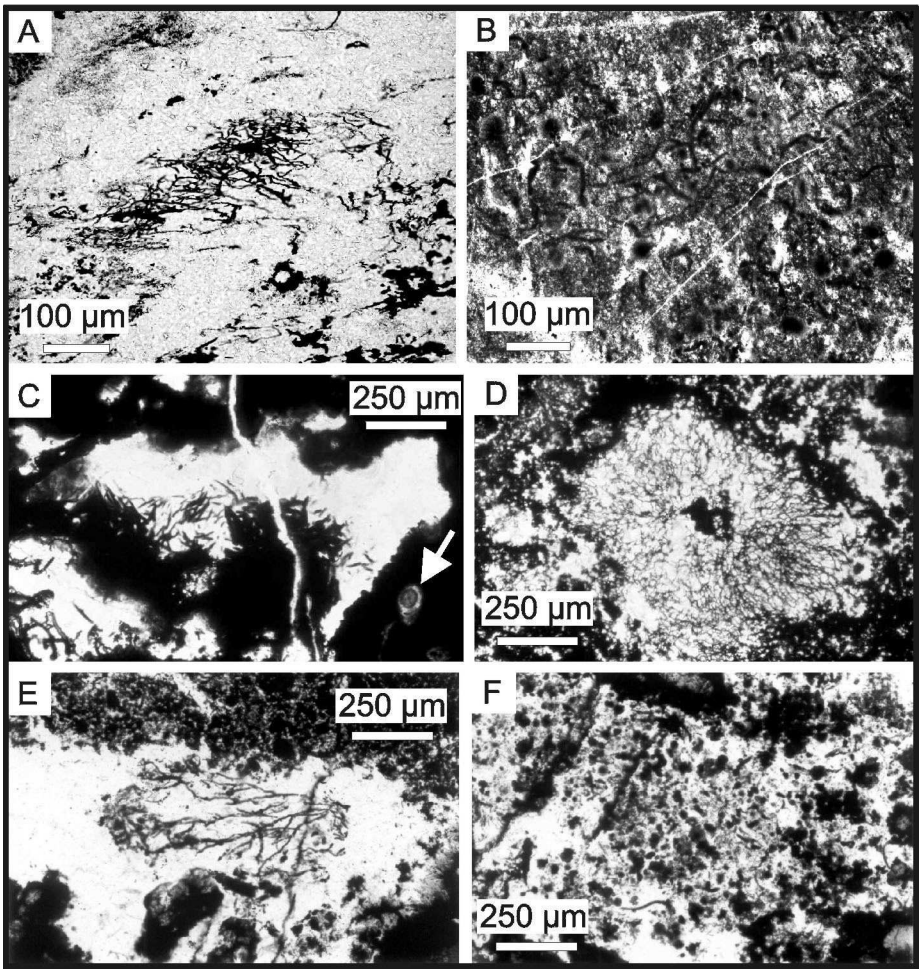

Figure 4. Jasper microtextures; transmitted light photomicrographs. (A) Filaments in hematite poor lamina, Høydal jasper. (B) Filaments in hematite-rich lamina; Høydal jasper. (C) Filaments in quartz domains surrounded by hematite-rich matrix; Alexandrinka jasper. Note late stage quartz vein cross cutting both microtextures and diagenentic spherule (white arrow). (D) Radiating filaments; Ballynoe jasper. (E) Dendritic filaments in quartz domain; Figueroa jasper. (F) Hematite spherules and filaments; Figueroa jasper.

terminal knobs (Figure 6G). A proportion of the Ballynoe filaments have a distinctive twisted morphology (Figure 6A, B; Boyce, Little, and Russell 2003, Figure 5B). The branched filaments (which includes both twisted and nontwisted forms) often recombine at intervals to form loose networks, most of which have a random orientation, but some radiate out from a central mass and some are orientated roughly parallel to laminae (Figures 4A–D, 6A, B; Juniper and Fouquet 1988, Figure 4; Alt et al. 1992, Figure 6B, C; Duhig et al. 1992a, Figure 2A, B; Boyce et al. 2003, Figure 5). In the Barlo, Coast Range ophiolite and Figueroa jaspers some of the small filaments are aggregated into spherical structures (Juniper and Fouquet 1988, Figure 4C, D). Structurally the small jasper filaments are hollow or silica filled cylinders with walls formed by a coating of submicron scale crystals of hematite (or Fe-oxyhydroxide in the ODP Core 129-801C-4R jasper) (Figure 6C, D, H). Using acid etched samples Duhig et al. (1992a, Figure 3A, B) showed that the hematite crystals forming the Mount Windsor filament coatings are interlocking, and some have their c axes orientated parallel to the filament elongation. The thickness of the hematite coatings is variable, with the coating thickness generally increasing with filament diameter. Some of the filaments in the Ballynoe and Løkken jaspers have such sparse coatings of hematite crystals that they are almost invisible (Figure 6H). Some of Løkken filaments (type II filaments of Grenne and Slack 2003b) are structurally more complex in that small hematite coated filaments (type I filaments of Grenne and Slack 2003b) are overgrown by silica and then another coating of hematite to form tubular structures.

The other filament type in the Kambia, Figueroa, Ballynoe, and Mount Windsor jaspers are those that form dendritic branching structures (Figures 5, 7). These dendritic structures have very regularly spaced, fractal-looking geometries and show

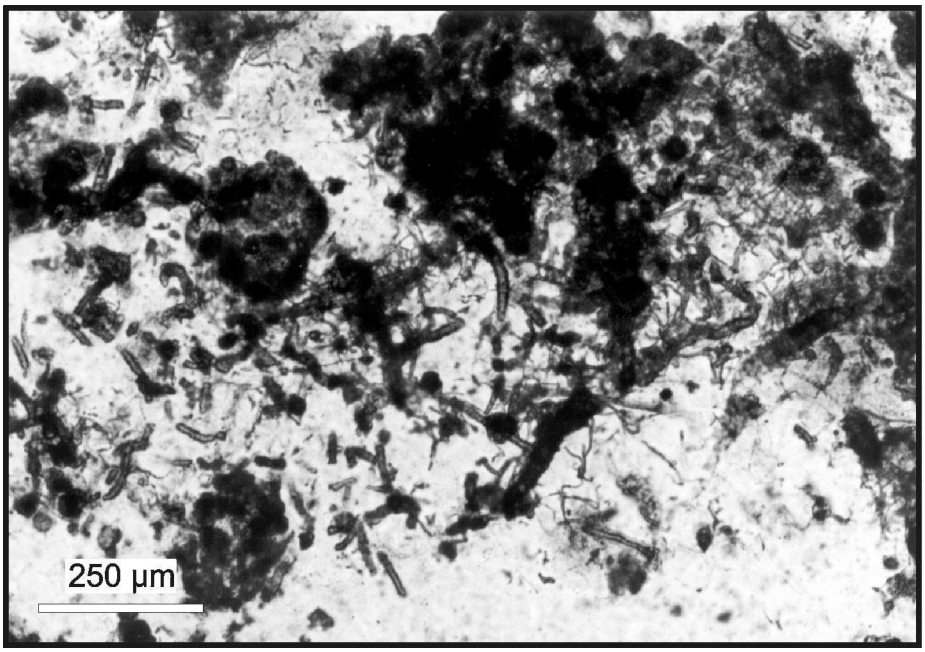

Figure 5. Figueroa jasper; transmitted light photomicrographs. Note close association of hematite spherules, large filaments and small filaments in quartz matrix.

obvious directed growth patterns originating from laminae or central points (Figure 7A–D). The individual filaments forming the dendritic structures differ from the small filaments as they have greater diameters (>15 μm), are generally longer (up to 5,000 μm), have thicker coatings of hematite, and branch at more regular intervals. The dendritic structures are usually less numerous than the small filaments, except in the Ballynoe jasper where they occupy more than twice the volume of the small filaments. Also associated with the dendritic structures in the Ballynoe jasper are large sinusoidal filaments upon which small hematite dendrites grow (Figure 7E, G). These structures do not appear to be cylindrical but rather laminae. The hematite dendritic structures are contemporaneous with the small filaments. The small filaments usually occur around and within the dendritic structures but are distinct from them. However, in a few cases in the Ballynoe jasper groups of small filaments can be seen to give rise directly to dendritic structures (Figure 7F).

DISCUSSION

Biogenicity of the Jasper and TAG Fe Oxide Filaments

The jasper filaments and TAG filaments share many morphological characteristics: (1) they have similar sizes, (2) they are concentrated in discrete laminae or domains, (3) they have a range of straight, twisted, branching and dendritic forms, (4) some have directed growth patterns parallel to sedimentary laminae, and (5) they are formed of cylinders of Fe oxides (mostly hematite). This indicates the modern TAG filaments and ancient jasper filaments were formed by similar processes.

The smaller jasper filaments and most of the TAG filaments also share many of these characteristics with the Fe oxide filaments found in the hydrothermal Fe oxide deposits listed in Table 1. For example, the twisted filaments in the TAG samples and the Ballynoe jasper are identical to those Fe oxide filaments attributed to the Fe oxide encrusted twisted stalks of *Gallionella* spp. in deep water (Alt 1988; Boyd and Scott 2001; Emerson and Moyer 2002; Kennedy et al. 2003a, 2003b, 2003c) and shallow water (e.g., Hanert 1973, 2002) hydrothermal vent sites, and weathered sulfide mineral surfaces (Edwards et al. 2003a). Similarly many of the other jasper and TAG filaments are like the filaments attributed to the Fe oxide-encrusted sheaths of *Leptothrix ochracea* (e.g., Alt 1988; Emerson and Revsbech 1994; Boyd and Scott 2001; Emerson and Moyer 2002; Kennedy et al. 2003a, 2003b, 2003c) and those formed by the bacterial strain PV-1 (Emerson and Moyer 2002). The branching jasper and TAG filaments may record true branching of filamentous microbes or the successive budding of separate microbial cells (termed "false branching"), a phenomenon known to produce bifurcating stalks in *Gallionella* spp. (e.g., Heldal and Tumyr 1983) and sheaths in *Sphaerotilus natans* (e.g., Ghiorse 1984).

Other small jasper filament morphologies could be attributed to microbial structures: small filament aggregations in the Barlo, Coast Range ophiolite and Figueroa jaspers are similar to filament aggregations found in the Coriolis Troughs Fe oxide deposits (Iizasa et al. 1998) and those formed by the bacterial strain PV-1 (Emerson and Moyer 2002), and the terminal knobs on some of small Figueroa filaments are like the attachment structures of *Leptothrix* sheaths. The septae in the very small filaments in the Figueroa and Mount Windsor jaspers could

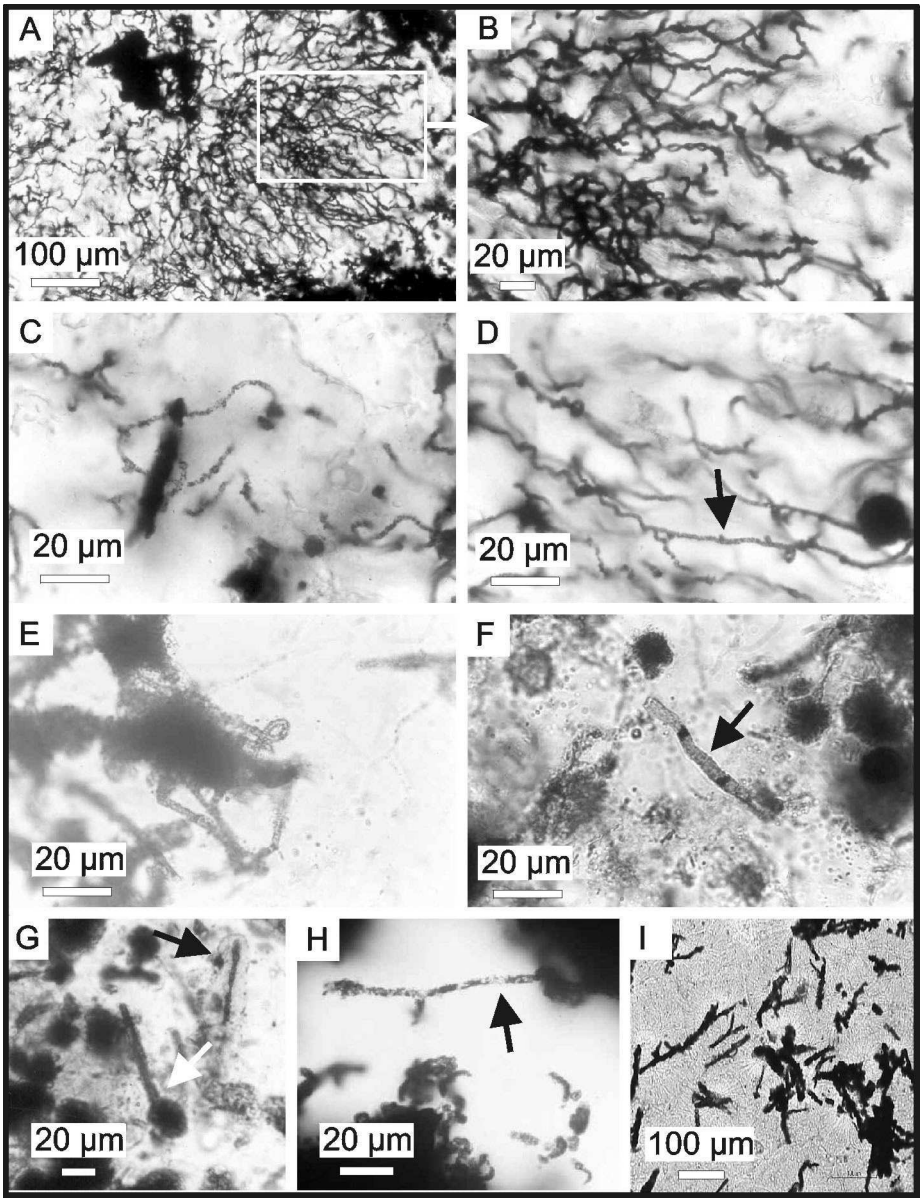

Figure 6. Small jasper filaments; transmitted light photomicrographs. (A) Twisted filaments forming radiating network; Ballynoe jasper. (B) Detail of (A). (C) Curved filaments with sparse hematite coatings; Ballynoe jasper. (D) Coiled and straight filaments; arrow points to 'bud' structure. Ballynoe jasper. (E) Looped filament; Figueroa jasper. (F) Septate filament; Figueroa jasper. (G) Filament with terminal knob. Arrow points to hematite filament coated in early stage quartz. Figueroa jasper. (H) Straight filament growing from hematite-rich matrix into quartz. Arrow points to area of sparse hematite coating on filament. Alexandrika jasper. (I) Branching filaments in chalcedony matrix; Kambia jasper.

represent junctions between cells in an Fe encrusted sheath and might therefore be compared with the Fe-oxidizing bacterium *Sphaerotilus natans* that forms chains of cells within a sheath (Ghiorse 1984).

The implication of the identification of the small jasper filaments as fossils of the Fe oxidizing bacteria *Gallionella*, *Leptothrix*, and *Sphaerotilus* is that these jaspers were formed from low temperature, near neutral pH, low $f(O_2)$ and ferrous iron-rich vent fluid, as these are the optimal living conditions for these bacteria (e.g., Boyd and Scott 2001).

The large dendritic filaments in the TAG gypsum cemented samples and the Kambia, Figueroa, Ballynoe, and Mount Windsor jaspers are very like the dendritic Fe oxide filamentous textures in Fe oxide-silica deposits in the Indian Ocean (Halbach et al. 2002), on the EPR (Juniper and Fouquet 1988, Figures 6A, 8) and at TAG (Hopkinson et al. 1998); (Table 1),

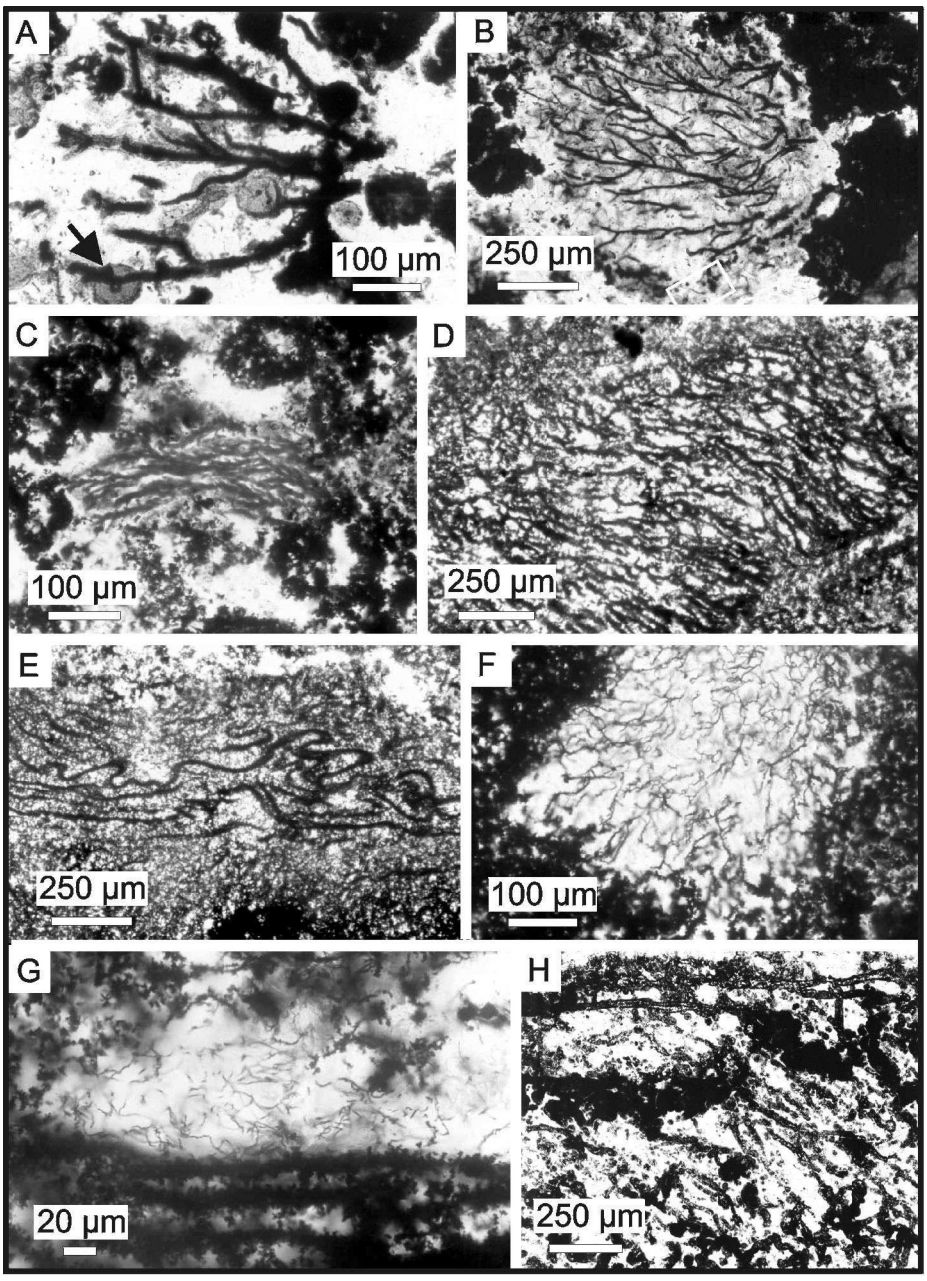

Figure 7. Large jasper filaments; transmitted light photomicrographs. (A) Sparsely branched dendrite growing from discrete point; Figueroa jasper. Arrow points to quartz sphere (probably with some Fe) forming on filament branch. (B) Sparsely branched dendrite growing from discrete point; Figueroa jasper. White rectangle (bottom center) corresponds to area shown in Figure 6F. (C) Pectinate dendrites; Ballynoe jasper. (D) Lamina of pectinate dendrites; Ballynoe jasper. (E) Large sinusoidal filaments among dendrites; Ballynoe jasper. (F) Domain of small filaments that pass laterally into dendrites; Ballynoe jasper. (G) Small filaments associated with sinusoidal filaments (lower third) and dendrites (top third); Ballynoe jasper. (H) Large straight and branched filaments; Høydal jasper.

none of which have been attributed to specific microbial morphologies. There are two competing hypotheses to explain the formation of these structures. Juniper and Fouquet (1988) suggested they are microbial in origin and represent dense Fe oxide deposition on filaments in the most oxidized zones of microbial mats. In contrast, Hopkinson et al. (1998) proposed an abiogenic mechanism where the dendrites are the result of diffusion limited growth of branching Fe-aggregates in a silica gel at the dissolution-redox front associated with pyrite weathering.

Definitive proof for the biogenic origin of the TAG and jasper filaments would be finding bacterial cells or remnant organic matter inside the hematite cylinders, as has been shown in other modern Fe oxide filaments (Fortin et al. 1998; Emerson and Moyer 2002; Kennedy et al. 2003a, 2003b, 2003c). Unfortunately this proof is lacking at present; organic material could not be detected within the Figueroa filaments by Laser Raman spectroscopy (Little and Thorseth 2002). However, the lack of organic matter may not be of great significance, because in modern Fe oxide deposits the volume of living cells or organic carbon may be very low compared to the volume of empty Fe oxide encrusted sheaths (Juniper and Fouquet 1988; Boyd and Scott 2001). For example, only 7% of Fe oxide encrusted *Leptothrix* sheaths in ground spring water in Denmark contained living cells (Emerson and Revsbech 1994).

Without the evidence of organic matter the identification of the TAG and jasper Fe oxide filaments (and most of the other filaments examples listed in Table 1) as biogenic or abiogenic structures rests on morphology alone, with all the inherent problems associated with this methodology (e.g., Reysenbach and Cady 2001; García-Ruiz et al. 2002, 2003). As discussed previously, many of the TAG and jasper filaments are identical to various structures formed by Fe-oxidizing bacteria. However, as abiogenic mechanisms for Fe oxide filament formation have been proposed (Hopkinson et al. 1998; García-Ruiz et al. 2002, 2003), these must also be considered. Abiogenic mechanisms must explain the formation of hollow cylinders of Fe oxides, in some cases with the Fe oxide crystals not being in contact with each other; straight, twisted, branching and dendritic morphologies; internal septae and terminal knobs; and directed growth patterns. García-Ruiz et al. (2002, 2003) have been able to grow abiogenic witherite (barium carbonate) structures, for example twisted filaments, in alkaline silica solutions that superficially look very like some of the Fe oxide filaments (García-Ruiz et al. 2002, Figure 1D, E, 2B–E; García-Ruiz et al. 2003, Figure 1). However, apart from the fact the physicochemical conditions are radically different, these biomorphs differ from the TAG and jasper filaments in several important ways: (1) the initial biomorphs are formed of solid witherite, not cylinders of Fe oxides (although García-Ruiz et al. 2003 were able to produce hollow helical silica filaments by acid etching the witherite), (2) most are an order of magnitude larger than the Fe oxide filaments, and (3) there are no "biomorphs" that are truly septate, like the Figueroa and Mount Windsor filaments, nor are there any that are looped morphologies (Figure 6E) or branching networks (Figure 6A, B, I).

Two of the lines of evidence used by Hopkinson et al. (1998) to support their model for the formation of the TAG dendritic textures in highly viscous silica gels was that there are no cavities between the Fe oxyhydroxide dendrites, these being filled entirely with silica, and that the dendrites do not project beyond the silica cement into free space. However, the lack of silica cement in our TAG Fe oxide filament meshes, and very similar filaments (indicating same formation processes) cemented by both silica and gypsum in our TAG samples, does not conform to this model of abiogenic filament growth in a silica gel. In addition the gypsum which cements Fe oxide filaments in the TAG sediments has $\delta^{34}S_{(CDT)}$ values of +9.6–11.35‰ indicating that the SO_4^{2-} is derived from sulfide oxidation (average sediment bulk sulfide $\delta^{34}S_{(CDT)} = +7.5‰$) (Glynn unpublished data) rather than seawater ($\delta^{34}S_{(CDT)} = +21‰$). Due to the high solubility of sulfate in seawater the presence of sulfide derived sulfate is unexpected and requires precipitation of the sulfate before mixing and dilution by sediment porewaters can occur. Since gypsum is highly undersaturated in the sediment porewaters, inorganic homogeneous precipitation of gypsum is unlikely. However, meshes of bacterial filaments growing directly from oxidation of mineral dissolution products on sulfide surfaces creates a geochemical microenvironment at the mineral/porewater interface where free advective and diffusive exchange with bulk seawater are restricted (e.g., Thompson and Ferris 1990; Schultze-Lam, Harauz, and Beveridge 1992). In these conditions, the saturation level of gypsum could be increased by continual addition of SO_4^{2-} from sulfide decay to the bacterial mesh, where filament surfaces act as nucleation sites. Precipitation via heterogeneous nucleation on bacterial filaments requires a lower saturation level than that required for homogeneous nucleation from a fluid. Effectively, bacterially promoted nucleation is energetically favored over abiogenic precipitation (Warren and Ferris 1998). The presence of Fe oxide filaments within gypsum and the intimate association with FeS_2 oxidation supports a bacteriogenic origin for these structures. Furthermore, the dendritic textures figured by Hopkinson et al. (1998) are not cylinders of Fe oxides like the small jasper and our TAG filaments. This indicates that our TAG filaments and those in the jaspers are non-diffusive structures and are therefore most likely to have biogenic origins. This interpretation supports previous reports of supposed microbial fossils from within the TAG deposit (Al-Hanbali, Sowerby, and Holm 2001; Al-Hanbali and Holm 2002). Whether the large sinusoidal filaments in the Ballynoe jasper, and the large dendritic filaments in the TAG gypsum cemented samples and the Kambia, Figueroa, Ballynoe and Mount Windsor jaspers are biogenic structures is less certain; these structures could be abiogenic as they do not correspond closely to known microbial forms. However, as noted above, some of the small Ballynoe filaments that we interpret to be biogenic, are directly connected to large dendritic filaments (Figure 7F). This transition between small filaments and larger Fe oxide rich dendrites is also seen in EPR Fe oxides (Juniper and Fouquet 1988, Figure 6A), and could represent abiogenic Fe oxide growth onto preformed biogenic Fe oxides (Emerson and Moyer 2002).

Although we have identified a bacteriogenic component in the formation of the TAG metalliferous sediment samples and the ancient jaspers, it must be noted that Fe oxide filaments of all morphologies make up only a percentage of the total volume of Fe oxides in all the studied material, usually much less than half. The rest of the Fe oxides occur as small spherules and larger amorphous masses that are apparently contemporaneous

with the Fe oxide filaments (Figures 4F, 5, 6E–G). The amorphous masses in particular are a strong indication that abiogenic precipitation of Fe oxides is also important in the formation of Fe oxide deposits, supporting the contention of Boyd and Scott (2001). It is difficult to estimate the relative proportions of abiogenic and bacteriogenic Fe oxide precipitation from our samples as it is very likely that the metabolic activity of even volumetrically small colonies of Fe oxidizing bacteria will alter the local physiochemical conditions enough to substantially increase the precipitation of Fe oxides than would occur by abiogenic precipitation alone (Sobolev and Roden 2001; Emerson and Moyer 2002; Kennedy et al. 2003a, 2003b, 2003c). To resolve this issue quantitative experiments using living Fe oxidizing bacteria need to be performed.

The Fe oxide filaments discussed here are very similar to filaments from Tertiary to Devonian volcanic rocks, oxidized orebodies, solution cavities in limestones, and impact melt rock reviewed by Hofmann and Farmer (2000), and interpreted by them to have formed subsurface.

Microbial Fossilization Processes

Based on our observations of the TAG and jasper filaments, and previous work on biogenic Fe oxide production, we propose the following fossilization process. (1) Nucleation of nanometric-scale Fe oxide particles (probably poorly ordered Fe oxyhydroxides) on the cell wall surfaces/organic sheaths of Fe-oxidizing bacteria (e.g., *Letpothrix*) and the stalks of *Gallionella*, as a direct consequence of the metabolic oxidation of Fe(II) to Fe(III) and/or by sorption of preformed Fe(III) colloids (Fortin et al. 1998; Warren and Ferris 1998; Banfield et al. 2000; Glasauer et al. 2001). (2) Initially these coatings of Fe oxide particles were sparse, but with increasing Fe oxide production the coatings thickened to enclose whole cells/stalks in a cylinder of Fe oxides. The bacteria may then have moved out of the sheaths/released the stalks to leave mineralized structures. (3) The mineralized sheaths and stalks may then have acted as nucleation sites for abiogenic Fe oxide mineralization forming dendritic structures. (4) The Fe oxide microbial fossils then acted as frameworks for colloidal silica formation (and gypsum at TAG). Later thermal maturation of the silica and the bacteriogenic Fe oxides produced minerals such as quartz, chalcedony, geothite and hematite, and the syneresis textures seen in all the jaspers (Duhig et al. 1992a, 1992b; Grenne and Slack 2003b).

CONCLUSIONS

Based on morphological similarities with structures formed by Fe oxidizing bacteria, we believe that the small jasper filaments and most of the TAG filaments are biogenic structures and were most probably formed by a variety of Fe oxidizing bacteria, including *Gallionella* and *Leptothrix*. The large dendritic filaments in the jaspers and TAG samples have equivocal origins. The implication is that a variety of Fe oxide filament morphologies in jaspers are direct evidence for bacteriogenic Fe oxide precipitation at hydrothermal vent sites back at least to the early Ordovician, 490 million years ago, and that a proportion of jaspers associated with massive sulfide deposits formed from low temperature, near neutral pH, low $f(O_2)$ and ferrous iron-rich vent fluid. These filament morphologies can therefore be used as biomarkers for bacteriogenic Fe oxide precipitation in Proterozoic and Archaean rocks on Earth, and possibly on other planets as well (e.g., Mars).

REFERENCES

Al-Hanbali H, Holm NG. 2002. Evidence for fossilized subsurface microbial communities at the TAG hydrothermal mound. Geomicro J 19: 429–438.

Al-Hanbali H, Sowerby S, Holm NG. 2001. Biogenicity of silicified microbes from a hydrothermal system: relevance to the search for evidence of life on earth and other planets. Earth Planet Sci Lett 191:213–218.

Alt JC. 1988. Hydrothermal oxide and nontronite deposits on seamounts in the Eastern Pacific. Mar Geol 81:227–239.

Alt JC, France-Lanord C, Floyd PA, Castillo P, Galy, A. 1992. Low temperature hydrothermal alteration of Jurassic ocean crust, site 801. Proc Ocean Drilling Program, Scientific Results 129:415–427.

Alt JC, Lonsdale P, Haymon R, Muehlenbachs K. 1987. Hydrothermal sulfide and oxide deposits on seamounts near 21°N, East Pacific Rise. Geol Soc Am Bull 98:157–168.

Banfield JF, Welch SA, Zhang H, Thomsen Ebert T, Lee Penn R. 2000. Aggregation-based crystal growth and microstructure development in natural iron oxyhydroxide biomineralization products. Science 289:751–754.

Barrett TJ, Taylor PN, Lugowski J. 1987. Metalliferous sediments from DSDP leg 92: The East Pacific Rise Transect. Geochim Cosmochim Acta 51:2241–2253.

Bau M, Dulski P. 1999. Comparing yttrium and rare earths in hydrothermal fluids from the Mid-Atlantic Ridge: implications for Y and REE behaviour during near-vent mixing and for the Y/Ho ratio of Proterozoic seawater. Chem Geol 155:77–90.

Binns RA, Scott SD, Bogdanov YA, Lisitzin AP, Gordeev VV, Gurvich EG, Finlayson EJ, Boyd T, Dotter LE, Wheller GE, Muravyev KG. 1993. Hydrothermal oxide and gold-rich sulfate deposits of Franklin Seamount, Western Woodlark Basin, Papua New Guinea. Econ Geol 88:2122–2153.

Bogdanov YA, Gorshov AI, Bogdanova OY, Gurvich EG, Sivtsov AV. 1998. Composition of low-temperature Fe-Mn minerals in metalliferous sediments of the TAG area (Mid-Atlantic Ridge). Okeanologiya 38:11–121. [Russian text, English abstract.]

Bogdanov YA, Lizitzin AP, Binns, Gorshov AI, Gurvich EG, Dritz VA, Dubinina GA, Bogdanova OY, Sivtsov AV, Kuptsov VM. 1997. Low-temperature hydrothermal deposits of Franklin Seamount, Woodlark Basin, Papua New Guinea. Mar Geol 142:99–117.

Boyce AJ, Little CTS, Russell MJ. 2003. A new fossil vent biota in the Ballynoe Barite Deposit, Silvermines, Ireland: evidence for intracratonic seafloor hydrothermal activity about 352 Ma. Econ Geol 98:649–656.

Boyd TD, Scott SD. 2001. Microbial and hydrothermal aspects of ferric oxyhydroxides and ferrosic hydroxides: the example of Franklin Seamount, Western Woodlark Basin, Papua New Guinea. Geochem Trans 7. [Internet Journal.]

Cornell RM, Schwertmann U. 1996. The Iron Oxides: Structure, Properties, Reactions, Occurrence and Uses. Germany: VHC. 573p.

Davidson GJ, Stolz AJ, Eggins SM. 2001. Geochemical anatomy of silica iron exhalites: evidence for hydrothermal oxyanion cycling in response to vent fluid redox and thermal evolution (Mt. Windsor Subprovince, Australia. Econ Geol 96:1201–1226.

Duhig NC, Davidson GJ, Stolz J. 1992a. Microbial involvement in the formation of Cambrian sea-floor silica-iron oxide deposits, Australia. Geology 20:511–514.

Duhig NC, Stolz J, Davidson GJ, Large RR.1992b. Cambrian microbial and silica gel textures in silica iron exhalites from the Mount Windsor volcanic belt, Australia: their petrography, chemistry, and origin. Econ Geol 87:764:784.

Edwards KJ, McCollom TM, Konishi H, Buseck PR. 2003a. Seafloor bioalteration of sulfide minerals: results from in situ incubation studies. Geochim Cosmochim Acta 67:2843–2856.

Edwards K, Rogers D, Wirsen CO, McCollom TM. 2003b. Isolation and characterization of novel psychrophilic, neutrophilic, Fe-oxidizing, chemolithautotrophic α and γ proteobacteria from the deep sea. Appl Environ Microbiol 69:2906–2913.

Emerson D, Moyer CL. 2002. Neutrophilic Fe-oxidizing bacteria are abundant at the Loihi Seamount hydrothermal vents and play a major role in Fe oxide deposition. Appl Environ Microbiol 68:3085–3093.

Emerson D, Revsbech NP. 1994. Investigation of an iron-oxidizing microbial mat community located near Aarhus, Denmark: field studies. Appl Environ Microbiol 60:4022–4031.

Fortin D, Ferris FG, Scott S. 1998. Formation of Fe-silicates and Fe oxides on bacterial surfaces in samples collected near hydrothermal vents on the Southern Explorer Ridge in the northeast Pacific Ocean. Am Min 83:1399–1408.

García-Ruiz JM, Carnerup A, Christy AG, Welham NJ, Hyde ST. 2002. Morphology: an ambiguous indicator of biogenicity. Astrobiology 2:353–369.

García-Ruiz JM, Hyde ST, Carnerup AM, Christy AG, Van Kranendonk MJ, Welham NJ. 2003. Self-assembled silica-carbonate structures and detection of ancient microfossils. Science 302:1194–1197.

Ghiorse WC. 1984. Biology of iron and manganese depositing bacteria. Ann Rev Microbiol 38:515–550.

Glasauer S, Langley S, Beveridge TJ. 2001. Sorption of Fe (hydr)oxides to the surface of *Shewanella putrefaciens*: cell-bound fine-grained minerals are not always formed de novo. Appl Environ Microbiol 67:5544–5550.

Grenne T, Slack JF. 2003a. Paleozoic and Mesozoic silica-rich seawater: Evidence from hematitic chert (jasper) deposits. Geology 31:319–322.

Grenne T, Slack JF. 2003b. Bedded jaspers of the Ordovician Løkken ophiolite, Norway: seafloor deposition and diagenetic maturation of hydrothermal plume-derived silica-iron gels. Min Dep 38:625–639.

Halbach M, Halbach P, Lüders V. 2002. Sulfide-impregnated and pure silica precipitates of hydrothermal origin from the Central Indian Ocean. Chem Geol 182:357–375.

Halbach M, Koschinsky A, Halbach P. 2001. Report on the discovery of *Gallionella ferruginea* from an active hydrothermal field in the deep sea. InterRidge News 10:18–20.

Hanert HH. 1973. Rezente marine eisenerze auf Santorin, Griechenland II. Bakterogenese von eisenhydroxidsedimenten. Geol Rund 62:803–812.

Hanert HH. 2002. Bacterial and chemical iron oxide deposition in a shallow bay on Palaea Kameni, Santorini, Greece: microscopy, electron probe microanalysis, and photometry of in situ experiments. Geomicrobiol J 19:317–342.

Hannington M, Jonasson I. 1992. Fe and Mn oxides at seafloor hydrothermal vents. Catena Supplement 21:351–370.

Hekinian R, Hoffert M, Larqué P, Cheminée JL, Stoffers P, Bideau D. 1993. Hydrothermal Fe and Si oxyhydroxide deposits from South Pacific intraplate volcanoes and East Pacific Rise axial and off-axial regions. Econ Geol 88:2099–2121.

Heldal M, Tumyr O. 1983. Gallionella from metalimnion in an eutrophic lake: morphology and X-ray energy-dispersive microanalysis of the apical cells and stalks. Can J Mircobiol 29:303–308.

Herzig PK, Becker KP, Stoffers P, Backer H, Blum N. 1988. Hydrothermal silica chimney fields in the Galapagos Spreading Center at 86°W. Earth Planet Sci Lett 89:73–86.

Hofmann BA, Farmer JD. 2000. Filamentous fabrics in low-temperature mineral assemblages: are they fossil biomarkers? Implications for the search for a subsurface fossil record on the early Earth and Mars. Planet Space Sci 48:1077–1086.

Holm NG. 1987. Biogenic influences on the geochemistry of certain ferruginous sediments of hydrothermal origin. Chem Geol 63:45–57.

Hopkinson L, Roberts S, Herington R, Wilkinson J. 1998. Self-organisation of submarine hydrothermal siliceous deposits: evidence from the TAG hydrothermal mound, 26N Mid-Atlantic Ridge. Geology 26:347–350.

Iizasa K, Kawasaki K, Maeda K, Matsumoto T, Saito N, Hirai K. 1998. Hydrothermal sulfide-bearing Fe-Si oxyhydroxide deposits from the Coriolis Troughs, Vanuatu backarc, southwestern Pacific. Mar Geol 145:1–21.

James R, Elderfield H. 1996. Chemistry and ore-forming fluids and mineral formation rates in an active hydrothermal sulfide deposit on the Mid-Atlantic Ridge. Geology 24:1147–1150.

Juniper SK, Fouquet Y. 1988. Filamentous iron-silica deposits from modern and ancient hydrothermal vents. Can Mineral 26:859–869.

Juniper SK, Sarrazin J. 1995. Interaction of vent biota and hydrothermal deposits: present evidence and future experimentation. In: Humphris SE, Zierenberg RA, Mullineaux LS, Thompson RE, editors. Seafloor Hydrothermal Systems: Physical, Chemical, Biological, and Geological Interactions. Geophys Mono 91. Washington, DC: American Geophysical Union. p 178–193.

Kennedy CB, Scott SD, Ferris FG. 2003a. Characterization of bacteriogenic iron oxide deposits from Axial Volcano, Juan de Fuca Ridge, Northeast Pacific Ocean. Geomicrobiol J 20:199–214.

Kennedy CB, Scott SD, Ferris FG. 2003b. Ultrastructure and potential subseafloor evidence of bacteriogenic iron oxides from Axial Volcano, Juan de Fuca Ridge, north-east Pacific Ocean. FEMS Microbiol. Ecol. 43:247–254.

Kennedy CB, Martinez RE, Scott SD, Ferris FG. 2003c. Surface chemistry and reactivity of bacteriogenic iron oxides from Axial Volcano, Juan de Fuca Ridge, north-east Pacific Ocean. Geobiology 1:59–69.

Köhler B, Singer A, Stoffers P. 1994. Biogenic nontronite from marine white smoker chimneys. Clays and Clay Minerals 42:698–701.

Konhauser KO. 1998. Diversity of bacterial iron mineralization. Earth Sci Rev 43:91–121.

Koski RA, Lonsdale PF, Shanks WC, Berndt ME, Howe SS. 1985. Mineralogy and geochemistry of a sediment hosted hydrothermal sulfide deposit from the Southern Trough of the Guaymas Basin, Gulf of California. J Geophys Res 90:6695–7607.

Lalou C, Thompson G, Arnold M, Brichet E, Druffel E, Rona PA. 1990. Geochemistry of TAG and Snakepit hydrothermal fields, Mid-Atlantic Ridge: witness to a long and complex hydrothermal history. Earth Planet Sci Lett 97:113–128.

Little CTS, Herrington RJ, Haymon RM, Danelian T. 1999. Early Jurassic hydrothermal vent community from the Franciscan Complex, San Rafael Mountains, California. Geology 27:167–170.

Little CTS, Thorseth IH. 2002. Hydrothermal vent microbial communities: a fossil perspective. Cah Biol Mar 43:317–319.

Millero F, Sotolongo S, Izaguirre M. 1987. The oxidation-kinetics of Fe(II) in seawater. Geochim Cosmochim Acta 51:793–801.

Mills R, Clayton T, Alt JC. 1996. Low-temperature fluid flow through sulfidic sediments from TAG: modification of fluid chemistry and alteration of mineral deposits. Geophys Res Lett 23:3495–3498.

Mills RA, Elderfield H, Thomson J. 1993. A dual origin for the hydrothermal component in a metalliferous sediment core from the Mid-Atlantic Ridge. J Geophys Res 98:9671–9681.

Palmer M, and scientific party. 1996. Cruise report. The interaction of microbial activity and diagenesis in hydrothermal sediments at the Mid Atlantic Ridge at 26°N. University of Bristol, Department of Geology. p 1–26.

Reysenbach A-L, Cady S. 2001. Microbiology of ancient and modern hydrothermal systems. Trends in Microbiology 9:79–86.

Rona PA, Hannington M, Raman CV, Thompson G, Tivey MK, Humphris SE, Lalou C, Petersen S. 1993. Active and relict seafloor hydrothermal mineralisation at the TAG hydrothermal field, Mid-Atlantic Ridge. Econ Geol 88:1989–2017.

Rona PA, Klinkhammer G, Nelsen TA, Trefry JH, Elderfield H. 1986. Black smokers, massive sulphides and vent biota at the Mid-Atlantic Ridge. Nature 321:33–37.

Schultze-Lam S, Harauz G, Beveridge TJ. 1992. Participtation of a cyanobacterial S-layer in fine grain mineral formation. J Bacteriol 174:7971–7981.

Severmann S, Mills RA, Palmer MR, Fallick AE. 2004. The origin of clay minerals in active and relict hydrothermal deposits. Geochim Cosmochim Acta. In press.

Sobolev D, Roden EE. 2001. Suboxic deposition of ferric iron by bacteria in opposing gradients of Fe(II) and oxygen at circumneutral pH. Appl Environ Microbiol 67:1328–1334.

Stoffers P, Glasby GP, Stüben D, Pierre TG, Webb J, Cardile CM. 1993. Comparative mineralogy and geochemistry of hydrothermal iron-rich crusts from the Pitcairn, Teahitia-Mehetia, and Macdonald hot spot areas of the S.W. Pacific. Mar Georesources Geotechnol 11:45–86.

Thompson J, Ferris F. 1990. Cyanobacterial precipitation of gypsum, calcite and magnesite from natural alkaline lake water. Geology 18:995–998.

Thorseth IH, Torsvik T, Torsvik V, Daae FL, Pedersen RB, Keldysh–98 Scientific party. 2001. Diversity of life in ocean floor basalt. Earth Planet Sci Lett 194:31–37.

Warren L, Ferris F. 1998. Continuum between sorption and precipitation of Fe(II) on microbial surfaces. Environ Sci Technol 32:2331–2337.